




Investigation of the elemental partitioning behaviour and site preference in ternary model nickel-based superalloys by atom probe tomography and first-principles calculations

S. H. Liu, C. P. Liu, W. Q. Liu, X. N. Zhang, P. Yan & C. Y. Wang


To cite this article: S. H. Liu, C. P. Liu, W. Q. Liu, X. N. Zhang, P. Yan & C. Y. Wang (2016) Investigation of the elemental partitioning behaviour and site preference in ternary model nickel-based superalloys by atom probe tomography and first-principles calculations, Philosophical Magazine, 96:21, 2204-2218, DOI: [10.1080/14786435.2016.1192298](https://doi.org/10.1080/14786435.2016.1192298)

 View supplementary material 

 Published online: 29 Jun 2016.

 Submit your article to this journal 

 Article views: 92

 View related articles 

 View Crossmark data 

Investigation of the elemental partitioning behaviour and site preference in ternary model nickel-based superalloys by atom probe tomography and first-principles calculations

S. H. Liu^{a,b}, C. P. Liu^c, W. Q. Liu^d, X. N. Zhang^c, P. Yan^e and C. Y. Wang^{b,e}

^aSchool of Materials Science and Engineering, Tsinghua University, Beijing, China; ^bDepartment of Physics, Tsinghua University, Beijing, China; ^cInstitute of Microstructure and Property of Advanced Materials, Beijing University of Technology, Beijing, China; ^dKey Laboratory for Microstructures, Shanghai University, Shanghai, China; ^eCentral Iron and Steel Research Institute, Beijing, China

ABSTRACT

The topologically close-packed phase formation is heavily influenced by the concentrations of Co, Ru, and Cr in Ni-based superalloys. For this purpose, we investigate the partitioning behaviour and site preference of these additions in the model Ni–Al–X single crystal superalloys by atom probe tomography and first-principles calculations. Compared with the commercial multicomponent superalloys, Co and Ru still strongly partition to the γ phase, while Cr weakly partitions to the γ phase in the ternary model alloys. Based on the γ' phase composition analyses, Ru and Cr atoms preferentially substitute for the Al sublattice sites, whereas Co atoms substitute at both Al and Ni sublattice sites in the ordered γ' -Ni₃Al phase. First-principles calculations on the substitutional formation energies at 0 K were performed to understand the site preference, and the partitioning coefficient of additions was given in a quantitative model. The partitioning behaviour and site preference of Co, Ru, and Cr by theoretical calculations are consistent with the experimental results.

ARTICLE HISTORY

Received 21 Apr 2016
Accepted 16 May 2016

KEYWORDS

Nickel-based superalloys; atom probe tomography (APT); partitioning coefficient; first-principles calculations

1. Introduction

Nickel-based superalloys with excellent high-temperature strength and creep resistance have been widely used as turbine blades in jet propulsion and electricity generation [1,2]. After decades of ongoing effort to enhance the temperature capability of the superalloys, the turbine entry temperature has been raised, thereby leading to an improved fuel economy of turbines with reduced carbon emissions [1]. The unique microstructure of Ni-based single crystal superalloys contains a high-volume fraction of γ' -Ni₃Al(L1₂) strengthening phases, which are coherently embedded in a solid solution of strengthening γ -Ni(fcc) matrix phases. A wide variety of alloying elements are added to enhance the high-temperature properties of each phase. For example, cobalt, chromium, ruthenium, molybdenum, tungsten, and rhenium prefer to partition to the γ phase, while aluminium, titanium, and tantalum promote the formation of the γ' ordered phase [3–10]. It is well

accepted that the thermal stability, γ/γ' lattice misfit, morphology, and volume fraction of γ' precipitates are closely related to the concentration of alloying elements in both phases. Among the major alloying elements, Co is reported to stabilise the material microstructure [11,12], and reduce the γ' solvus temperature [11,13]. Ru, as a characteristic element for the fourth-generation single crystal superalloys, suppresses the topologically close-packed (TCP) phase formation, stabilise the material's microstructure during operation, and effectively improves the creep performance [7,14,15]. Ru and Co additions could decrease the stacking fault energy and influence the deformation mechanism of higher-generation superalloys [16,17]. Cr is known to play a critical role in improving the hot corrosion and oxidation resistance owing to the formation of a Cr_2O_3 protective coating [3,18]. Preventing TCP formation for the latest generation superalloys requires a low Cr content. However, the Cr content can also be too low to protect against oxidation, although this can also be prevented by coating the blades [1]. In addition, Cr has been reported to reduce the γ' solvus temperature and the anti-phase boundary energy (γ_{APB}) of the γ' phase [19].

The concentrations of Co, Ru, and Cr in the γ phases are related to the formation of TCP and stacking faults as well as the lattice misfits and precipitate morphologies. Therefore, it is instructive to consider the partitioning of these elements to the γ and γ' phases, which is critical to the mechanical properties of Ni-based superalloys at elevated temperature. The partitioning behaviour of refractory elements (e.g. Ta, W, Re, Mo) has already been investigated in model and commercial multicomponent Ni-based superalloys using an electron probe X-ray microanalysis (EPMA) [5], atom probe tomography (APT) [4,6,20–22], and transmission electron microscopy [8,9]. These efforts have shown the different partitioning behaviour of refractory elements between the model and commercial multicomponent superalloys. Similarly, the phase preference of Co, Ru, and Cr for model alloys should be studied, as this would influence the thermal stability, morphology and other factors associated with the elevated temperature mechanical properties. Using experimental techniques and theoretical simulations, Co is shown to partition to the γ phase and substitutes for the Ni sublattice sites in the γ' phase in the commercial multicomponent superalloys [23–26], and Ru is observed to partition to the γ phase and occupies the Al sublattice sites in quaternary superalloys [20,27]. However the partition behaviours of Co and Ru have not been investigated in ternary model single crystal alloys. Cr has been reported to partition to the γ phase in ternary model superalloys [28,29]; however, it is unclear whether Cr occupies the Ni or Al sublattice sites [23,25,30–33]. Similarly, the sites occupied by Co are also unclear [23,34–36], as the site preference of alloying elements would alter its own partitioning behaviour [20,22,32,37]. Therefore, a correct interpretation of the experimental data is of vital importance for this controversial topic.

Early experimental efforts have focused on the polycrystalline alloy ingots, and have shown the ingots to mainly be quaternary. Owing to the importance of the subsystems of superalloys, systematic studies of elemental partitioning behaviour at the nanoscale for ternary model single crystal superalloys should be carried out, which would add to the knowledge-based for alloy design. In this study, we have investigated the site preference and partitioning behaviour of Co, Ru, and Cr across the γ/γ' interface in model Ni–Al–X single crystal superalloys, employing both APT and first-principles calculations. Based on the measured elemental partitioning, the effects of the additions on the microstructure of γ' also are also discussed.

Table 1. Compositions of the ternary model alloys investigated in this work.

Alloy (wt.%)	Al	Co	Ru	Cr	Ni
Ni–Al	8.8	–	–	–	Bal.
Ni–Al–Co	8.8	5.8	–	–	Bal.
Ni–Al–Ru	8.7	–	3.0	–	Bal.
Ni–Al–Cr	8.2	–	–	3.0	Bal.

2. Experimental and theoretical methods

2.1. Materials preparation and experimental techniques

The nominal compositions of the model Ni-based alloys investigated in this work are listed in Table 1. Cast ingots were prepared by vacuum induction melting. The master ingots were then directionally solidified using the Bridgman technique (2 mm/min withdrawal rate) to form $\langle 001 \rangle$ -oriented single crystals. The single crystal bars were homogenised to eliminate chemical segregation at 1330 °C for 20 h, and subsequently aged at 870 °C for 32 h to produce a homogeneous distribution of cubic γ' phase. All bars were cooled with water after annealing unless otherwise stated.

The microstructure of ternary alloys was investigated using an FEI Quanta 600 scanning electron microscope at the voltage of 20 kV. The SEM samples were prepared by mechanical polishing and electrochemical corrosion in a solution of 48% (volume fraction) H_2SO_4 , 40% HNO_3 and 12% H_3PO_4 with a dwell time of 10 s at room temperature.

The degree of elemental microsegregation was measured by EPMA (JXA-8230, JEOL, Japan) X-ray mapping to quantify the homogenisation of the heat treated alloy. The samples used for EPMA were prepared according to standard metallographic techniques. The beam conditions were 20 kV and 10 nA. The map area was $810 \mu\text{m} \times 810 \mu\text{m}$.

The elemental partitioning behaviour between the γ and γ' phases was analysed by APT. APT specimens were prepared by cutting $0.5 \text{ mm} \times 0.5 \text{ mm} \times 15 \text{ mm}$ rods from the heat treated single crystal bars, before the standard two-step electro-polishing procedures[38]. In the first step, all rods were electrochemically polished in an electrolyte of 25% (volume fraction) perchloric acid and 75% acetic acid at 20V DC; fine-polishing was then performed in a 2% perchloric acid in butoxyethanol solution at 10–20 V DC to form microtips with a radius of curvature $\sim 50 \text{ nm}$. APT microtips were performed in a voltage-pulsed local-electrode atom probe (LEAP 3000 HR), at a microtip temperature of $\sim 50 \text{ K}$, a gauge pressure of $\sim 10^{-8} \text{ Pa}$, a pulse repetition rate of 200 kHz and a pulse voltage fraction of 20%. The detection efficiency of the instrument is 36%. Results were analysed using the IVAS 3.6.8 software, and the compositional information was obtained by employing the proximity histogram (proxigram) methodology [39].

2.2. Computational methodology

The structural and energetic properties were studied based on first-principles calculations of the total energies. These calculations employed Vienna *ab initio* simulation package [40,41] was employed using the projector augmented wave method [42,43] and the general gradient approximation in the Perdew–Burke–Ernzerhof form [44]. The energy cutoff for the plane wave basis set was 350 eV. A first-order Methfessel–Paxton smearing method

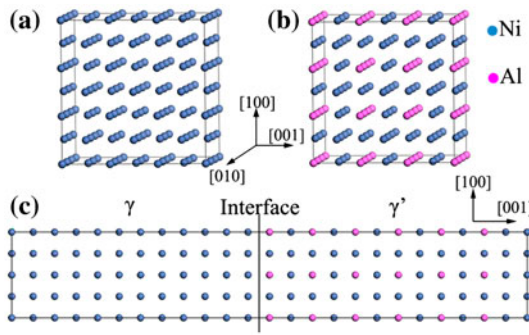


Figure 1. (colour online) Morphology and atomic structure of γ -Ni and γ' -Ni₃Al in ternary model alloys for the simulation of supercell models. The cyanine and magenta circles denote Ni and Al atoms, respectively. (a) The γ -phase is approximated by a fcc lattice containing $3 \times 3 \times 3$ Ni unit cells. (b) The γ' -phase is approximated by a L1₂ lattice containing $3 \times 3 \times 3$ Ni₃Al unit cells. (c) The ternary model alloy is approximated by a $2 \times 2 \times 12$ supercell consisting of 192 atoms.

[45] was used with a searing width of SIGMA = 0.2 eV. The convergence accuracy of the total energies was 10^{-5} eV in the relaxation of the electronic degrees of freedom. The lattice parameters of γ -Ni and γ' -Ni₃Al in the DFT calculations were 3.516 and 3.569 Å, respectively. Since there is a small lattice mismatch between a_γ and $a_{\gamma'}$, we used the coherent structure to deal with the problem encountered by first-principles methods using periodic boundary conditions. The effect of lattice parameter on defect energies was investigated in the supplemental material. By changing the lattice parameter from 3.516 to 3.569 Å, our total energy calculations show that the coherent lattice parameter is 3.545 Å at the stable interface.

For the single-phase system, the supercells of γ -Ni and γ' -Ni₃Al were both $3 \times 3 \times 3$ supercells consisting of 108 atoms; the Brillouin zone integration used was the $5 \times 5 \times 5$ Monkhorst-Pack [46] k -point scheme. For the two-phase system, a $6 \times 6 \times 2$ k -point mesh and a $2 \times 2 \times 12$ supercell consisting of 192 atoms were used. To eliminate the interactions of parallel γ/γ' interfaces, we introduced a vacuum region of 12 Å to separate the interfaces. The two-phase system has two subcells: the γ -subcell contains $2 \times 2 \times 6$ fcc unit cells (96 atoms), and the γ' -subcell contains $2 \times 2 \times 6$ L1₂ unit cells (96 atoms). Both subcells are situated adjacent to each other to form a coherent γ/γ' interface (0 0 1) [22,37]. Figure 1 illustrates the three models introduced above.

It is known that the reliability of first-principles calculations depends on the k -point sampling and the simulation cell size. To check the above factors, we plotted the values of interest as functions of the k -point mesh and cell size (N_{atom}^{-1}). As shown in Figure 2(a), $5 \times 5 \times 5$ k -point sampling for single-phase system was deemed sufficient for convergence. Figure 2(b) shows the effect of the cell size on the substitution formation energy (E_{sub}) for cobalt in both the fcc-Ni and L1₂-Ni₃Al structures. Based on three cell sizes, $2 \times 2 \times 2$, $3 \times 3 \times 3$, and $4 \times 4 \times 4$, it can be seen that the size-effect error for E_{sub} is small for both the fcc and L1₂ systems, suggesting that the $3 \times 3 \times 3$ supercell is sufficient to reduce the error in the single-phase system. We also do not find a significant difference between the results calculated for the $2 \times 2 \times 2$ and $3 \times 3 \times 3$ cells. Therefore, the calculation results have a reasonable convergence accuracy within a reasonable computational time in our $2 \times 2 \times 12$ simulation cell for a two-phase system. Thus, the dilute alloys are considered as

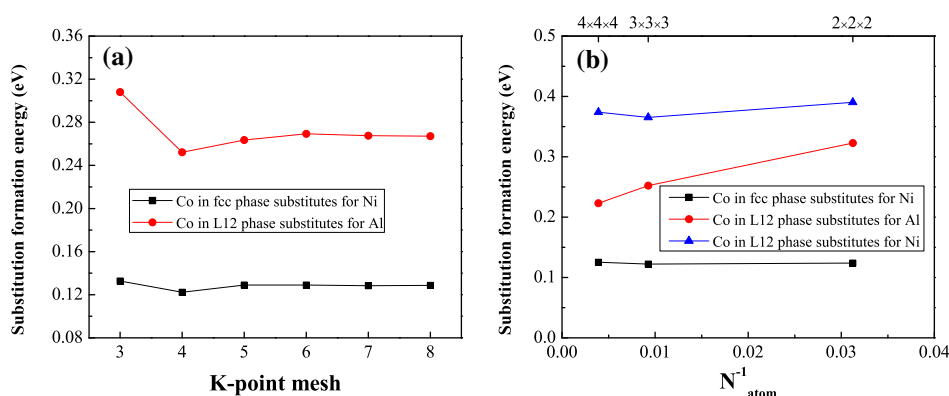


Figure 2. (colour online) Results of the convergence test performed on fcc Ni and $L1_2$ Ni_3Al with the Co impurity. The substitution formation energies (E_{sub}) are obtained by the variation of (a) Monkhorst–Pack k -point mesh, and (b) cell size.

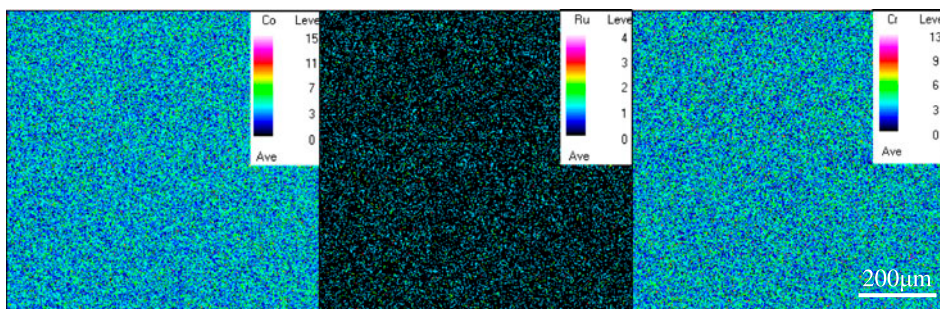


Figure 3. (colour online) EPMA maps of test materials after heat treatment for Co, Ru, and Cr.

a single doping model [47]; that is, there are no interactions between the impurities in two adjacent cells when placing many cells next to one another under the periodic boundary conditions.

All atomic positions were fully relaxed until the maximum Hellman–Feynman force was less than $0.02\text{eV}/\text{\AA}$ ($0.03\text{eV}/\text{\AA}$ for the $2 \times 2 \times 12$ supercell).

3. Results and discussion

3.1. Microstructure of the alloys

All the model alloys have been fully homogenised using the heat treatment procedures mentioned in Section 2.1. Co, Ru, and Cr are found to uniformly distribute in EPMA maps, as shown in Figure 3, indicating that no obvious dendritic microstructure or elemental microsegregation could be observed after the heat treatment. The mean sizes of the γ' precipitates are characterised by the average of the lengths of the precipitate's edges. In the Ni–Al and Ni–Al–Cr model alloys, shown in Figure 4, the γ' precipitates are almost rectangular, while the γ' precipitates of Ni–Al–Co and Ni–Al–Ru are cuboidal and spheroidal, respectively. Note that the shape of the precipitates is closely related to the γ/γ' misfit (the value of lattice misfit, δ) [48,49]. The misfit is calculated by the following equation:

Table 2. The size and morphology of γ' precipitates, and the lattice misfit.

Alloy	γ' size (μm)	γ' morphology	δ at R.T. Estimated (%)
Ni–Al	0.28	Nearly rectangular	0.60
Ni–Al–Cr	0.18	Nearly rectangular	0.65
Ni–Al–Co	0.25	Cuboidal	0.59
Ni–Al–Ru	0.23	Spheroidal	0.42

$$\delta = 2 \times \frac{a_{\gamma'} - a_{\gamma}}{a_{\gamma'} + a_{\gamma}} \quad (1)$$

where the lattice parameters in each phase (a_{γ} , $a_{\gamma'}$) depend on Vegard's law [50,51]. As the chemical segregation has been fully homogenised, the atomic fractions of elements in the γ and γ' phases in Vegard's formulas are used by the APT results in Section 3.2. The estimated values of the misfit are 0.60% (Ni–Al), 0.59% (Ni–Al–Co), 0.42% (Ni–Al–Ru), and 0.65% (Ni–Al–Cr). As the absolute magnitude of the misfit δ increases, the γ' precipitates transform from spherical to cubic, which agrees with Fahrman's [49] work. We propose that different alloying element content and partitioning behaviour lead to different degrees of misfit, thereby affecting the precipitate's shape. Furthermore, the morphology evolution of precipitates would affect the creep properties [51,52]. The size and morphology of γ' precipitates, as well as the lattice misfit, are given in Table 2.

3.2. Elemental partitioning between γ and γ' phases

The three-dimensional reconstruction in Figure 5 shows 17 at.% Al, 17 at.% Al, 17 at.% Al and 15 at.% Al isoconcentration surfaces indicating the interface between the γ and γ' phases for the model superalloys. The concentration profiles across the γ/γ' interface of elements using the proxigrams method are shown in Figure 6. The data indicate that Co and Ru clearly partition to the γ phase, whereas the partitioning tendency of Cr is rather negligible in a Ni–Al–Cr alloy. Numerically, the partitioning coefficient to characterise the phase preference of elements is defined by

$$K_M^{\gamma'/\gamma} = \frac{C_M^{\gamma'}}{C_M^{\gamma}} \quad (2)$$

where $C_M^{\gamma'}$ and C_M^{γ} are the atomic fractions of the M element in the γ' and γ phases, respectively. The compositions for each phase are accurately measured in sub-volumes which contain at least 1 million ions. Table 3 summarise the phase compositions of the three solute elements and the associated partitioning coefficient. Cr has a weaker tendency to partition to the γ phase with the partitioning coefficient $K_{\text{Cr}}^{\gamma'/\gamma} = 0.87$ than Co (0.40) and Ru (0.36). In all cases, $K_M^{\gamma'/\gamma} < 1$. Compared with the alloy RR2101, Co and Ru still strongly partition to the γ phase, while Cr weakly partitions to the γ phase in the ternary model alloys. The reason for the stronger partitioning tendency to the γ phase of Cr in the commercial multicomponent alloys is that there are many other alloying elements (Ta, W, Re, Ru, Co, Hf) added to the multicomponent alloy, while Cr is the only element in the ternary alloy. Other alloying additions would influence the solubility of Cr in both the γ and γ' phases. We can reasonably assume that the additions change the concentration

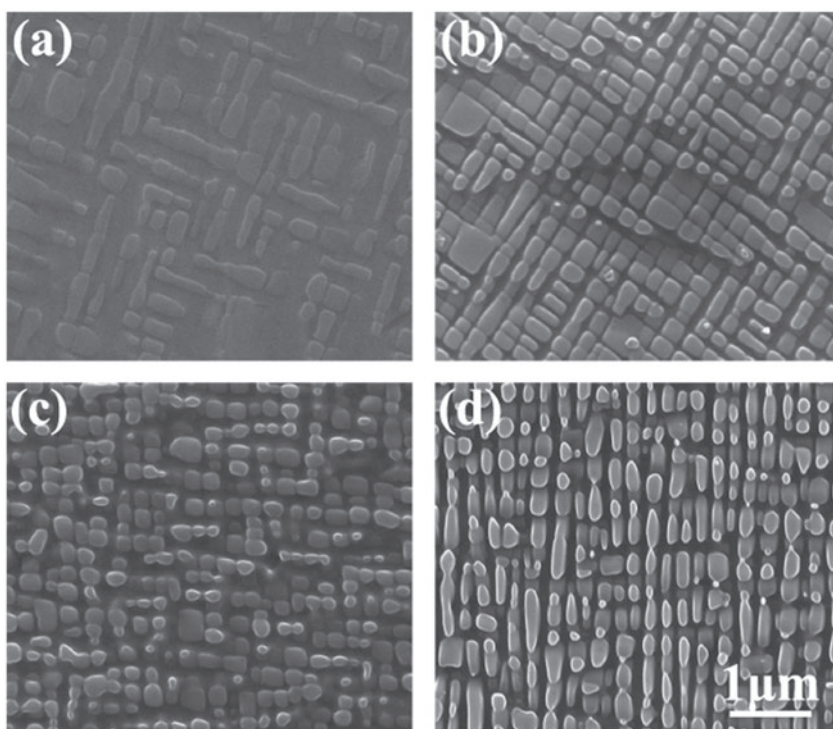


Figure 4. Secondary electron SEM images of the microstructure after ageing at 870 °C for 32h in (a) Ni–Al, (b) Ni–Al–Co, (c) Ni–Al–Ru, and (d) Ni–Al–Cr alloys. The light contrast reveals the γ' phase, while dark contrast indicates the γ phase channels that have been selectively etched.

Table 3. Phase compositions and partitioning coefficients $K_M^{\gamma'/\gamma}$.

Alloy	γ'/γ Composition at.(%)					Partitioning coefficients				
	Ni	Al	Co	Ru	Cr	Ni	Al	Co	Ru	Cr
Ni–Al	77.43/86.30	22.57/13.70	–	–	–	0.90	1.65	–	–	–
Ni–Al–Co	74.28/79.42	22.65/13.19	2.93/7.30	–	–	0.94	1.72	0.40	–	–
Ni–Al–Ru	76.22/83.71	23.04/14.20	–	0.75/2.08	–	0.91	1.62	–	0.36	–
Ni–Al–Cr	77.31/85.70	19.55/11.13	–	–	2.32/2.66	0.90	1.76	–	–	0.87
RR2101 [6]	66.09/46.02	16.55/3.08	8.79/26.65	0.88/2.90	1.34/9.50	1.44	5.37	0.33	0.30	0.14

of Cr in γ and γ' phases and sequentially change the partitioning coefficient. Especially, Ta is the element that partitions preferentially to the γ' phases and maybe responsible for displacing Cr from γ' phases into the γ -matrix. To test this hypothesis quantitatively, we performed first-principles calculations of the substitutional formation energy of Ta in Section 3.3.

Interestingly, the Al depletion region and Co pile-up zone emerge at the γ/γ' interface, as shown in the concentration profile in Figure 6. A similar phenomenon is also observed in Tan's [53] and Povstugar's [54] work. Although our Ni–Al–Co alloy was cooled with water after the ageing treatment, the cooling rate was limited. Hence, the local compositional effect during water-cooling is caused by elemental diffusion, which may not exist at high temperature (for example, the operation temperature of superalloys) [54]. However, no

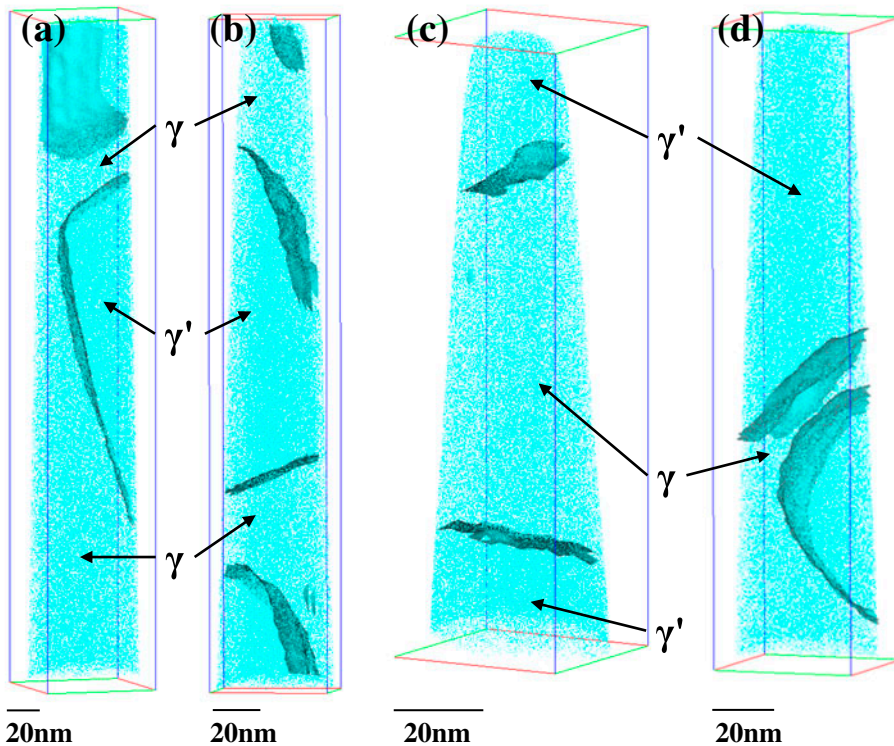


Figure 5. (colour online) Three-dimensional reconstructions acquired from: (a) Ni–Al binary alloy; (b) Ni–Al–Co ternary alloy; (c) Ni–Al–Ru ternary alloy; (d) Ni–Al–Cr ternary alloy. The γ/γ' interfaces are indicated by: (a) 17 at.% Al, (b) 17 at.% Al, (c) 17 at.% Al, and (d) 15 at.% Al isoconcentration surfaces. The Al atoms are represented in cyan, for clarity, other elements are not represented.

direct experimental proof to verify this is currently available. The compositional variations at the interfaces may influence the dislocations cutting the γ' phase and the migration of the interface during the rafting of the γ' phase in superalloys. At present, studies on these problems are in progress, and these results will be presented in a forthcoming paper.

Known for its anomalous yield effect, the intermetallic compound Ni_3Al is the critical strengthening phase of Ni-based superalloys for its high temperature mechanical properties. γ' - Ni_3Al is the typical ordered A_3B (L1_2 -type) structure, which consists of A-sublattice (the face centres) and B-sublattice (cube corner) with the ideal stoichiometry of 3:1. However, the binary phase diagram indicates that there is a small deviation (23–27 at.% Al) from the exact stoichiometry which must be accommodated by point defects [1]. This is remarkably consistent with our APT experimental results where the concentration of Al in the γ' is 22.57 at.% for the Ni–Al binary alloy (Table 3). Transition metal elements substituting at either Ni or Al sublattice sites show considerable solubility in Ni_3Al , which affects the mechanical properties of γ' - Ni_3Al [34]. The site occupancy behaviour of the transition metal elements in γ' - Ni_3Al is therefore not only of great interest but also quite useful for understanding their fundamental theoretical roles in γ' - Ni_3Al .

APT has been used to investigate the site preference of solute elements in Ni-based and Co-based alloys [20,32,54,55]. Thus, based on the binary Ni–Al alloy, in the case of the

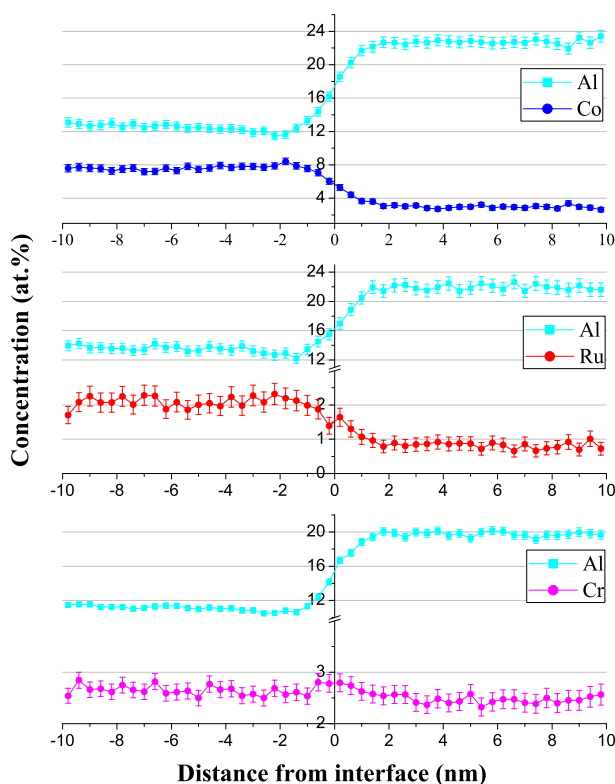


Figure 6. (colour online) Proximity histograms of the isoconcentration surfaces displayed in Figure 5 show the concentration profile of alloying elements: Al (cyan squares), Co (blue circles), Ru (red circles), and Cr (magenta circles). The partitioning of Al to the γ' phase is significant for all model alloys.

Ni–Al–Co alloy, the concentration sum of Al and Co in the γ' is 25.6 at.%, exceeding the reference value of 22.57 at.% and the stoichiometry characteristic value of 25 at.%, which indicates that Co occupies both Al and Ni sublattice sites in the ordered $L1_2$ structure. Similarly, for the Ni–Al–Ru alloy, the sum of Al content and Ru content in the γ' equals 23.8 at.%, indicating that the Ru substitutes preferentially to the Al sublattice sites. For the Ni–Al–Cr alloy, the sum of Al content and Cr content in the γ' equals 21.9 at.%, suggesting that Cr also substitutes preferentially to the Al sublattice sites. It is worth mentioning that the concentration sum of Al and Cr is less than the reference value 22.57 at.%, because some Ni atoms may substitute to the Al sites, resulting in anti-defects.

The highest spatial resolution of APT lies along the Z-axis, but the more direct proof for the preference of elements on the Al or Ni sites by layer-by-layer analysis of (0 0 2) planes of the $L1_2$ -Ni₃Al ordered phase is not currently available. The site preference of alloy elements is studied by first-principles calculations in Section 3.3.

3.3. First-principles calculations

Based on the single doping model hypothesis, no interactions are considered between alloying elements. When different alloying atoms (Co, Ru, and Cr) substitute for Ni or Al atoms at different positions from the γ/γ' interface, the total energies for different

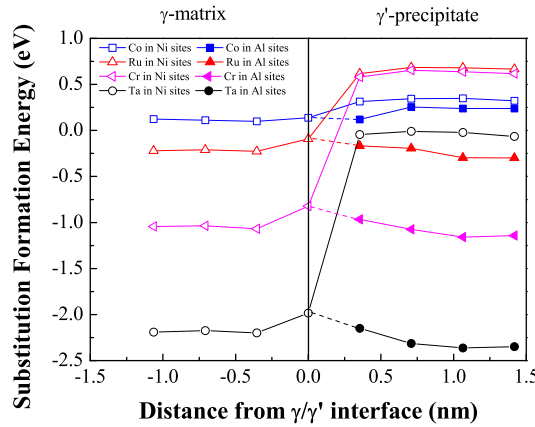


Figure 7. (colour online) The substitution formation energies of Co (blue squares), Ru (red up triangles), Cr (magenta left triangles), and Ta (black circles) as a function of distance from the γ/γ' interface depicted in Figure 1(c). The abscissa of each point on the graph represents an (0 0 1) atomic plane, where the γ/γ' interface is defined as the first atomic plane of the γ phase.

configurations are calculated. We also determine the total energies of the γ and γ' phases, when one alloying atom substitutes for Ni in the γ phase and for Ni or Al in the γ' phase. Therefore, we derive the substitutional formation energies of Co, Ru, and Cr as follows [20,56]:

$$E_{\text{sub,NiorAl}}^{\text{Min}\gamma'} = (E^{\text{Min}\gamma'} + \mu_{\text{Ni/Al}}) - (E^{\gamma'} + \mu_{\text{M}}) \quad (3)$$

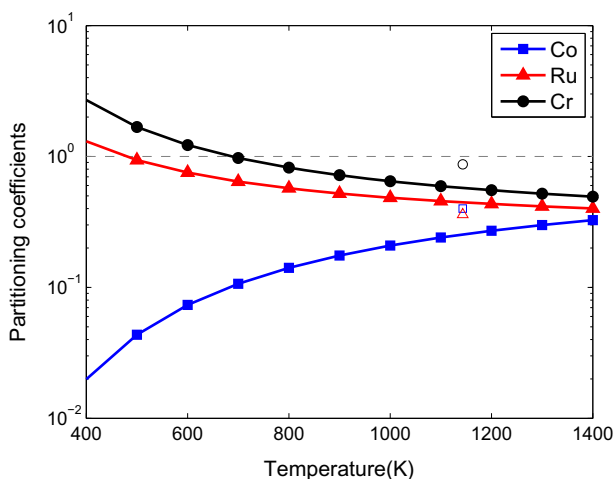
$$E_{\text{sub,Ni}}^{\text{Min}\gamma} = (E^{\text{Min}\gamma} + \mu_{\text{Ni}}) - (E^{\gamma} + \mu_{\text{M}}) \quad (4)$$

where M represents Co, Ru, and Cr, and $E_{\text{sub,NiorAl}}^{\text{Min}\gamma'}$ and $E_{\text{sub,Ni}}^{\text{Min}\gamma}$ are the total internal energies of the M-alloying supercells for substituting Ni or Al in γ' or γ , respectively. $\mu_{\text{Ni/Al}}$ is the chemical potential of Ni or Al in the bulk system. At the equilibrium state, μ_{Ni} is equal to the energy of per atom for bulk Ni, and the chemical potential (per unit) of bulk Ni_3Al is equal to $3\mu_{\text{Ni}} + \mu_{\text{Al}}$ [27,56], thus $\mu_{\text{Al}} = \mu_{\text{Ni}_3\text{Al}} - 3\mu_{\text{Ni}}$. μ_{M} is the chemical potential of alloying elements, and is calculated assuming the fcc structure. Figure 7 shows the substitution formation energies of Co, Ru, Cr, and Ta for different distances from the γ/γ' interface, which indicate that Ta has a stronger substitutional effect for Al sublattice sites of the γ' phases than Cr. These findings imply that Ta can replace Cr in the γ' phases, leading to a change of the partitioning coefficient of Cr between the two phases, as discussed in Section 3.2. For the single-phase system, the substitution formation energies are presented in Table 4. Comparing Figure 7 and Table 4, we note that the substitution energies of elements in the single-phase system are relatively close to the elements away from the γ/γ' interface in the two-phase system.

According to Figure 7 and Table 4, in the γ' phase, the substitution formation energies of Ru and Cr at Al sublattice sites are significantly smaller than those at the Ni sublattice; that is, Ru and Cr are energetically favourable to occupy the Al sublattice site. Unlike Ru and Cr, Co prefers Al or Ni sublattice sites, because the substitution formation energies of Co at Al sublattice sites are slightly smaller than those at Ni sublattice sites. This is consistent with our APT results. The substitution formation energies of Ru and Cr in the

Table 4. The substitution formation energies for Co, Ru, and Cr in the single-phase system.

Substitution formation energies (eV)	γ phase	γ' phase	
	substitution site for Ni	substitution site for Ni	substitution site for Al
Co	0.129	0.367	0.264
Ru	−0.142	0.676	−0.199
Cr	−0.932	0.539	−1.014

**Figure 8.** (colour online) The partitioning coefficient of Co (blue line), Ru (red line), and Cr (black line) as a function of temperature, calculated from Equation 5. The APT results of Co (blue open square), Ru (red open triangle), and Cr (black open circle) are also plotted for comparison.

γ' phase are slightly more negative than those in the γ phase; however, the results for Co are reversed. The differences (driving forces) between the substitution formation energies for Ni in the γ phase and for Al in the γ' phase show that Co tends to partition to the γ phase, while Ru and Cr tend to partition to the γ' phase. Nevertheless, the distribution behaviour of Ru and Cr maybe uncertain, because of insufficient 'driving forces' and only occupying 1/4 of Ni_3Al sublattice sites. To determine the accurate distribution tendency of alloying elements in the two phases, a model for the partitioning ratio is given [22].

$$K_M^{\gamma'/\gamma} \equiv \frac{C_M^{\gamma'}}{C_M^{\gamma}} = \frac{1}{4} \exp \left[-\frac{E_{\text{sub,Al}}^{\text{Min}\gamma'} - E_{\text{sub,Ni}}^{\text{Min}\gamma}}{k_B T} \right] \quad (5)$$

where $E_{\text{sub,Al}}^{\text{Min}\gamma'}$ and $E_{\text{sub,Ni}}^{\text{Min}\gamma}$ are the values from Equations (3) and (4), and the pre-exponential factor of 1/4 indicates that M (except Co) atoms only occupy Al sites in the γ' - Ni_3Al .

Equation (5) gives the quantitative partitioning trend of the alloying elements. If $K_M^{\gamma'/\gamma} > 1$, ternary additions trend to partition into the γ' phase; conversely, additions partition favourably to the γ phase if $K_M^{\gamma'/\gamma} < 1$. The partitioning coefficient of additions as a function of temperature is shown in Figure 8, and the experimental results performed by APT are also presented. The partitioning tendency of Co, Ru, and Cr obtained by calculation is consistent with the APT results, so the $K_M^{\gamma'/\gamma}$ values predicted are reasonably

accurate although there are some discrepancies with the absolute values. The possible reasons are as follows: (1) the previous theoretical classification of site preference is only strictly valid at 0 K, (2) solid solutions are ideal and dilute, (3) the entropy term is not included in the Equation (5).

4. Conclusion

By combining SEM, APT, and first-principles calculations, the phase partitioning of Co, Ru and Cr in different model Ni-based superalloys was studied. Through APT analyses for aged ternary Ni–Al–X alloys, the partition coefficients are $K_{\text{Co}}^{\gamma'/\gamma} = 0.40$, $K_{\text{Ru}}^{\gamma'/\gamma} = 0.36$, and $K_{\text{Cr}}^{\gamma'/\gamma} = 0.87$. Cr has a weaker tendency to partition to the γ phase in Ni–Al–Cr alloy than that in RR2101 superalloys because the other alloying additions change the partitioning coefficient of Cr. Ru and Cr preferentially substitute at the Al sublattice sites, whereas Co is likely to substitute at both Al and Ni sublattice sites in the ordered γ' -Ni₃Al phase. By performing first-principles calculations, the substitution formation energies of Ru and Cr at the Al sublattice sites are significantly smaller than at the Ni sublattice sites, whereas Co at Al sublattice sites is slightly smaller than at Ni sublattice sites in the γ' phase. The partitioning coefficient of additions at 870 °C is less than 1. The site preference and partitioning behaviour of Co, Ru, and Cr determined by calculation are consistent with the APT results.

Disclosure statement

The authors declare that there is no conflict of interests regarding the publication of this paper.

Funding

This work was supported by the National Basic Research Program of China [‘973 Project’, Ministry of Science and Technology of China, grant number 2011CB606402]; the simulations were carried out on the ‘Explorer 100’ cluster system of Tsinghua National Laboratory for Information Science and Technology, Beijing, China.

References

- [1] R.C. Reed, *The Superalloys: Fundamentals and Applications*, Cambridge University Press, Cambridge, 2006. Available at <http://dx.doi.org/10.1017/CBO9780511541285>.
- [2] T.M. Pollock and S. Tin, *Nickel-based superalloys for advanced turbine engines: Chemistry, microstructure and properties*, J. propul. power 22(2) (2006), pp. 361–374.
- [3] C.T. Sims, N.S. Stoloff, and W.C. Hagel, *superalloys II*, Wiley-Interscience, New York, NY, 1987.
- [4] P. Warren, A. Cerezo, and G. Smith, *An atom probe study of the distribution of rhenium in a nickel-based superalloy*, Mater. Sci. Eng., A 250(1) (1998), pp. 88–92.
- [5] T. Yokokawa, M. Osawa, K. Nishida, T. Kobayashi, Y. Koizumi, and H. Harada, *Partitioning behavior of platinum group metals on the γ and γ' phases of Ni-base superalloys at high temperatures*, Scr. Mater. 49(10) (2003), pp. 1041–1046.
- [6] R. Reed, A. Yeh, S. Tin, S. Babu, and M. Miller, *Identification of the partitioning characteristics of ruthenium in single crystal superalloys using atom probe tomography*, Scr. Mater. 51(4) (2004), pp. 327–331.

- [7] S. Walston, A. Cetel, R. MacKay, K. Ohara, D. Duhl, and R. Dreshfield, *Joint development of a fourth generation single crystal superalloy*, in *Superalloys 2004*, TMS Pennsylvania, 2004, pp. 15–24. Available at http://www.tms.org/Superalloys/10.7449/2004/Superalloys_2004_15_24.pdf.
- [8] A. Volek, F. Pyczak, R. Singer, and H. Mughrabi, *Partitioning of Re between γ and γ' phase in nickel-base superalloys*, *Scr. Mater.* 52(2) (2005), pp. 141–145.
- [9] B. Ge, Y. Luo, J. Li, and J. Zhu, *Study of γ/γ' interfaces in nickel-based, single-crystal superalloys by scanning transmission electron microscopy*, *Metall. Mater. Trans. A* 42(3) (2011), pp. 548–552.
- [10] J. Van Sluytman, A. La Fontaine, J. Cairney, and T. Pollock, *Elemental partitioning of platinum group metal containing Ni-base superalloys using electron microprobe analysis and atom probe tomography*, *Acta Mater.* 58(6) (2010), pp. 1952–1962.
- [11] G.L. Erickson, *Single crystal nickel-based superalloy*, US Patent 5,366,695, Nov 22, 1994.
- [12] W. Wang, T. Jin, J. Liu, X. Sun, H. Guan, and Z. Hu, *Role of Re and Co on microstructures and γ coarsening in single crystal superalloys*, *Mater. Sci. Eng. A* 479(1) (2008), pp. 148–156.
- [13] M. Nathal and L. Ebert, *The influence of cobalt, tantalum, and tungsten on the microstructure of single crystal nickel-base superalloys*, *Metall. Trans. A* 16(10) (1985), pp. 1849–1862.
- [14] A. Sato, H. Harada, T. Yokokawa, T. Murakumo, Y. Koizumi, T. Kobayashi, and H. Imai, *The effects of ruthenium on the phase stability of fourth generation Ni-base single crystal superalloys*, *Scr. Mater.* 54(9) (2006), pp. 1679–1684.
- [15] R. Hobbs, L. Zhang, C. Rae, and S. Tin, *Mechanisms of topologically close-packed phase suppression in an experimental ruthenium-bearing single-crystal nickel-base superalloy at 1100 °C*, *Metall. Mater. Trans. A* 39(5) (2008), pp. 1014–1025.
- [16] S. Ma, L. Carroll, and T. Pollock, *Development of γ phase stacking faults during high temperature creep of Ru-containing single crystal superalloys*, *Acta Mater.* 55(17) (2007), pp. 5802–5812.
- [17] X. Wang, J. Liu, T. Jin, and X. Sun, *The effects of ruthenium additions on tensile deformation mechanisms of single crystal superalloys at different temperatures*, *Mater. Des.* 63 (2014), pp. 286–293.
- [18] E.W. Ross and K.S. OHara, *Rene N4: A first generation single crystal turbine airfoil alloy with improved oxidation resistance, low angle boundary strength and superior long time rupture strength*, in *Superalloys 1996*, TMS Pennsylvania, 1996, pp. 19–25. Available at http://www.tms.org/superalloys/10.7449/1996/Superalloys_1996_19_25.pdf.
- [19] D.N. Duhl and A.D. Cetel, *Advanced high strength single crystal superalloy compositions*, US Patent 4,719,080, Jan 12, 1988.
- [20] Y. Zhou, Z. Mao, C. Booth-Morrison, and D.N. Seidman, *The partitioning and site preference of rhenium or ruthenium in model nickel-based superalloys: An atom-probe tomographic and first-principles study*, *Appl. Phys. Lett.* 93(17) (2008), p. 171905.
- [21] Y. Tu, Z. Mao, and D.N. Seidman, *Phase-partitioning and site-substitution patterns of molybdenum in a model Ni–Al–Mo superalloy: An atom-probe tomographic and first-principles study*, *Appl. Phys. Lett.* 101(12) (2012), p. 121910.
- [22] Y. Amouyal, Z. Mao, and D.N. Seidman, *Combined atom probe tomography and first-principles calculations for studying atomistic interactions between tungsten and tantalum in nickel-based alloys*, *Acta Mater.* 74 (2014), pp. 296–308.
- [23] D. Blavette, A. Bostel, and J. Sarrau, *Atom-probe microanalysis of a nickel-base superalloy*, *Metall. Trans. A* 16(10) (1985), pp. 1703–1711.
- [24] N. Wanderka and U. Glatzel, *Chemical composition measurements of a nickel-base superalloy by atom probe field ion microscopy*, *Mater. Sci. Eng. A* 203(1) (1995), pp. 69–74.
- [25] D. Collins, L. Yan, E. Marquis, L. Connor, J. Ciardiello, A. Evans, and H. Stone, *Lattice misfit during ageing of a polycrystalline nickel-base superalloy*, *Acta Mater.* 61(20) (2013), pp. 7791–7804.
- [26] H. Murakami, Y. Saito, and H. Harada, *Determination of atomistic structure of Ni-base single crystal superalloys using Monte Carlo simulations and atom-probe microanalyses*, in *Superalloys 1996*, TMS Pennsylvania, 1996, pp. 249–257. Available at http://www.tms.org/superalloys/10.7449/1996/Superalloys_1996_249_257.pdf.

- [27] X. Yu, C. Wang, X. Zhang, P. Yan, and Z. Zhang, *Synergistic effect of rhenium and ruthenium in nickel-based single-crystal superalloys*, J. Alloys Compd. 582 (2014), pp. 299–304.
- [28] C.K. Sudbrack, D. Isheim, R.D. Noebe, N.S. Jacobson, and D.N. Seidman, *The influence of tungsten on the chemical composition of a temporally evolving nanostructure of a model Ni–Al–Cr superalloy*, Microsc. Microanal. 10 (2004), pp. 355–365.
- [29] C. Booth-Morrison, J. Weninger, C.K. Sudbrack, Z. Mao, R.D. Noebe, and D.N. Seidman, *Effects of solute concentrations on kinetic pathways in Ni–Al–Cr alloys*, Acta Mater. 56(14) (2008), pp. 3422–3438.
- [30] M. Chaudhari, A. Singh, P. Gopal, S. Nag, G. Viswanathan, J. Tiley, R. Banerjee, and J. Du, *Site occupancy of chromium in the γ' -Ni₃Al phase of nickel-based superalloys: A combined 3d atom probe and first-principles study*, Philos. Mag. Lett. 92(9) (2012), pp. 495–506.
- [31] M. Enomoto and H. Harada, *Analysis of γ'/γ equilibrium in Ni–Al–X alloys by the cluster variation method with the Lennard–Jones potential*, Metall. Trans. A 20(4) (1989), pp. 649–664.
- [32] C. Booth-Morrison, Z. Mao, R.D. Noebe, and D.N. Seidman, *Chromium and tantalum site substitution patterns in Ni₃Al (112) γ' -precipitates*, Appl. Phys. Lett. 93(3) (2008), p. 033103.
- [33] S. Ochial, Y. Oya, and T. Suzuki, *Alloying behaviour of Ni₃Al, Ni₃Ga, Ni₃Si and Ni₃Ge*, Acta Metall. 32(2) (1984), pp. 289–298.
- [34] R.D. Rawlings and A.E. Staton-Bevan, *The alloying behaviour and mechanical properties of polycrystalline Ni₃Al (γ phase) with ternary additions*, J. Mater. Sci. 10(3) (1975), pp. 505–514.
- [35] J.S. Tiley, O. Senkov, G. Viswanathan, S. Nag, J. Hwang, and R. Banerjee, *A methodology for determination of γ site occupancies in nickel superalloys using atom probe tomography and x-ray diffraction*, Metall. Mater. Trans. A 44(1) (2013), pp. 31–38.
- [36] M. Miller and J. Horton, *Site occupation determinations by apfim for Hf, Fe, and Co in Ni₃Al*, Scr. Metall. 20(8) (1986), pp. 1125–1130.
- [37] Y.-J. Wang and C.-Y. Wang, *A first-principles survey of the partitioning behaviors of alloying elements on γ/γ' interface*, J. Appl. Phys. 104(1) (2008), p. 013109.
- [38] M.K. Miller, *Atom Probe Tomography: Analysis at the Atomic Level*, Springer Science and Business Media, 2012. doi:10.1007/978-1-4615-4281-0. Available at <http://www.springer.com/us/book/9780306464157>.
- [39] O.C. Hellman, J.A. Vandenbroucke, J. Rüsing, D. Isheim, and D.N. Seidman, *Analysis of three-dimensional atom-probe data by the proximity histogram*, Microsc. Microanal. 6(05) (2000), pp. 437–444.
- [40] G. Kresse and J. Hafner, *Ab initio molecular dynamics for liquid metals*, Phys. Rev. B 47 (1993), pp. 558–561.
- [41] G. Kresse and J. Furthmüller, *Efficient iterative schemes for ab initio total-energy calculations using a plane-wave basis set*, Phys. Rev. B 54 (1996), pp. 11169–11186.
- [42] P.E. Blöchl, *Projector augmented-wave method*, Phys. Rev. B 50 (1994), pp. 17953–17979.
- [43] G. Kresse and D. Joubert, *From ultrasoft pseudopotentials to the projector augmented-wave method*, Phys. Rev. B 59 (1999), pp. 1758–1775.
- [44] J.P. Perdew, K. Burke, and M. Ernzerhof, *Generalized gradient approximation made simple*, Phys. Rev. Lett. 77 (1996), pp. 3865–3868.
- [45] M. Methfessel and A.T. Paxton, *High-precision sampling for Brillouin-zone integration in metals*, Phys. Rev. B 40 (1989), pp. 3616–3621.
- [46] H.J. Monkhorst and J.D. Pack, *Special points for Brillouin-zone integrations*, Phys. Rev. B 13 (1976), pp. 5188–5192.
- [47] W. Chong-yu, L. Sen-ying, and H. Lin-guang, *Electronic structure of impurity (oxygen) stacking-fault complex in nickel*, Phys. Rev. B 41 (1990), pp. 1359–1367.
- [48] R. Ricks, A. Porter, and R. Ecob, *The growth of precipitates in nickel-base superalloys*, Acta Metall. 31(1) (1983), pp. 43–53.
- [49] M. Fährmann, P. Fratzl, O. Paris, E. Fährmann, and W.C. Johnson, *Influence of coherency stress on microstructural evolution in model Ni–Al–Mo alloys*, Acta Metall. Mater. 43(3) (1995), pp. 1007–1022.

- [50] P. Nash, *Phase Diagrams of Binary Nickel Alloys*, ASM International, 1991. Available at <https://books.google.com.hk/books?id=GfjUAAAAMAAJ>.
- [51] P. Caron, *High γ' solvus new generation nickel-based superalloys for single crystal turbine blade applications*, in *Superalloys 2000*, TMS Pennsylvania, 2000, pp. 737–746. Available at http://www.tms.org/superalloys/10.7449/2000/Superalloys_2000_737_746.pdf.
- [52] Y. Koizumi, T. Kobayashi, T. Yokokawa, J. Zhang, M. Osawa, H. Harada, Y. Aoki, and M. Arai, *Development of next-generation Ni-base single crystal superalloys*, in *Superalloys 2004*, TMS Pennsylvania, 2004, pp. 35–43. Available at http://www.tms.org/superalloys/10.7449/2004/Superalloys_2004_35_43.pdf.
- [53] X. Tan, D. Mangelinck, C. Perrin-Pellegrino, L. Rougier, C.-A. Gandin, A. Jacot, D. Ponsen, and V. Jaquet, *Atom probe tomography of secondary γ' precipitation in a single crystal Ni-based superalloy after isothermal aging at 1100 °C*, *J. Alloys Compd* 611 (2014), pp. 389–394.
- [54] I. Povstugar, P.-P. Choi, S. Neumeier, A. Bauer, C.H. Zenk, M. Goken, and D. Raabe, *Elemental partitioning and mechanical properties of Ti- and Ta-containing Co-Al-W-base superalloys studied by atom probe tomography and nanoindentation*, *Acta Mater.* 78 (2014), pp. 78–85.
- [55] S. Meher, H.-Y. Yan, S. Nag, D. Dye, and R. Banerjee, *Solute partitioning and site preference in γ/γ' cobalt-base alloys*, *Scr. Mater.* 67(10) (2012), pp. 850–853.
- [56] A.F. Kohan, G. Ceder, D. Morgan, and C.G. Van de Walle, *First-principles study of native point defects in ZnO*, *Phys. Rev. B* 61 (2000), pp. 15019–15027.